INSTITUTE OF PHYSICS PUBLISHING PLASMA SOURCES SCIENCE AND TECHNOLOGY
Plasma Sources Sci. Technol. **15** (2006) 1–12 UNCORRECTED PROOF

Evolution of charged species in propane/air flames: mass-spectrometric analysis and modelling

J M Rodrigues[1], A Agneray[1], X Jaffrézic[1], M Bellenoue[2], S Labuda[2], C Leys[3], A P Chernukho[4], A N Migoun[4], A Cenian[5], A M Savel'ev[6], N S Titova[6] and A M Starik[6]

[1] RENAULT-Technocentre, 1 av du Golf, 78288 Guyancourt cedex, France
[2] Laboratoire de Combustion et de Détonique, 1 av. Clément Ader, BP 40109, 86961 Futuroscope Chasseneuil Cedex, France
[3] Department of Applied Physics, Ghent University, Rozier 44, B-9000 Ghent, Belgium
[4] Heat and Mass Transfer Institute BASci., 15 Brovki str., 220072 Minsk, Belarus
[5] The Szewalski Institute of Fluid-flow Machinery, Polish Academy of Sciences, 80-952 Gdańsk, Fiszera 14, Poland
[6] Central Institute of Aviation Motors, 2 Aviamotornaya st., 111116 Moscow, Russia

E-mail: cenian@imp.gda.pl and star@ciam.ru

Received 8 February 2006, in final form 16 may 2006
Published
Online at stacks.iop.org/PSST/15

Abstract
The experimental and modelling studies of ion formation during combustion of propane/air mixtures are presented. The positive and negative ions mass/charge spectra in propane/air stoichiometric flame at atmospheric pressure are recorded in the range from 0 to 512 atomic mass units. The $C_2H_3O^+$ and HCO_2^- ions are found as the most abundant ionic species in the flame front region. By increasing the distance from the flame front the ion composition changes significantly. In the burnt gas region the H_3O^+, NO^+, CO_3^-, HCO_3^- ions are found as major charged species. To explain the experimental results the extended kinetic model describing the ion formation in flame and in extraction system of mass-spectrometer as well as ion–soot interaction is developed. It is shown that the ionic clusters, which are observed experimentally, form during the adiabatic expansion in the extraction system, and the presence of soot particles may change the total positive and the negative ion concentration in gas phase.

AQ1 (Some figures in this article are in colour only in the electronic version)

1. Introduction

In the past decades considerable interest has been shown in the investigation of non-equilibrium processes in combustion plasma that forms upon burning different hydrocarbons in air [1–12]. Such plasma in general is similar to the conventional dusty discharge plasma which indicates presence of a large amount of ions and electrons as well as carbon clusters and nanoparticles (soot particles) formed in the fuel rich region of diffusion flames or in combustors. Nevertheless, combustion plasma exhibits noticeable differences compared with other types of low temperature plasmas, such as the absence of an external electric field, the high rate of ion and electron production due to chemi-ionization reactions, the wide range of particle sizes (5–100 nm in diameter), the existence of both positively and negatively charged particles and the relatively small residence time of gaseous products and particles ($\tau_{res} \leqslant 100$ ms) in the high temperature ($T = 2000$–2500 K) region. The interest in studying combustion plasma is related to the significant environmental effects caused by the emission of combustion exhausts [13–15] and to the possible application of ion probes in controlling combustion and increasing burning efficiency [16].

JNL: PSST PIPS: 218399 TYPE: SPE TS: NEWGEN DATE: 22/6/2006 EDITOR: VC

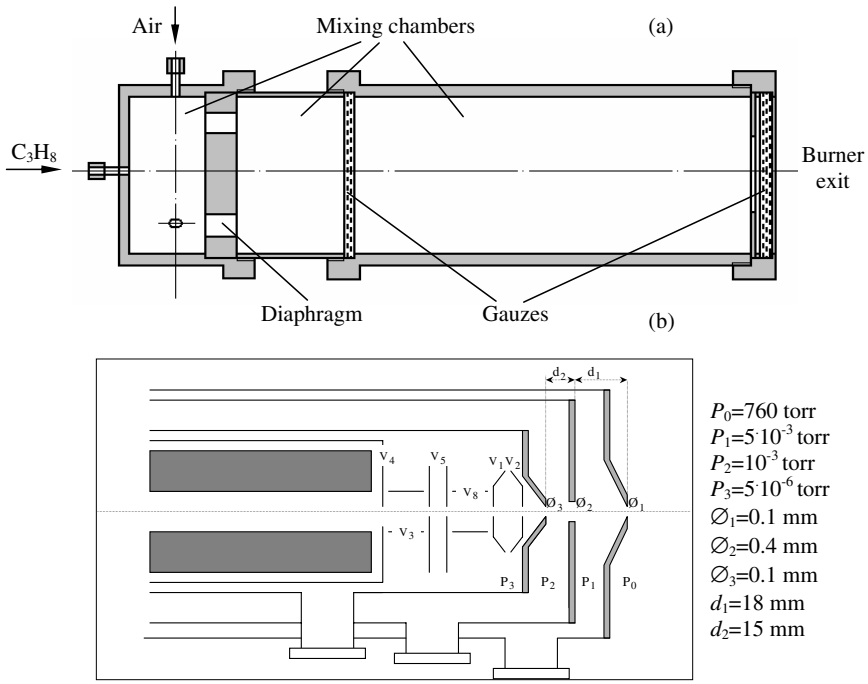

Figure 1. Schematic configuration of burner (*a*) and gas extraction set-up (*b*).

It is known that ions are strong aerosol precursors and enhance the growth of aerosol particles via ion-assisted coagulation [13]. Ions and electrons may attach themselves to soot particles, induce charge on their surface and stimulate the uptake of water molecules (or other dipole molecules) by soot particles [11], thereby increasing the ability of soot particles to act as cloud condensation nuclei.

Recent studies have demonstrated some prospective applications of ion probes to measure flame characteristics [16–18]. In particular, the local equivalence fuel/air ratio at the early stage of flame kernel development has been derived from ion probe measurements [16]. Calibrated probe signals have also been used to measure the quenching distance during head-on flame quenching [17]. The ionization probe technique combined with Schlieren diagnostics makes it possible to measure burning velocity in a model combustion chamber [18].

The further development and exploitation of ionization probe diagnostics and the understanding of environmental consequences of the emission of charged species and nanoparticles into the atmosphere is restrained by our limited knowledge of the flame ionization processes, of the evolution of ionic species concentrations in the post flame front region or in the combustor, of the interaction of combustion plasma with a probe and of soot particle charging. Therefore, extensive investigations (both experimental and numerical) related to combustion plasma formation and, in particular, to flame ion composition are required.

In this work a comprehensive study of ion formation during combustion of propane/air mixtures based on mass-spectrometric measurements as well as on numerical modelling of chemi-ionization processes is carried out. Also the clustering of ions that occurs during the transit of the gas through the extraction channel of the mass-spectrograph and its impact on the mass spectra are investigated.

2. Experimental set-up

A special burner was designed in order to study the charged species evolution in flames (see figure 1(*a*)). The burner is 150 mm in length and its inner diameter is 30 mm. Propane is injected into the mixing chamber through the channel 0.75 mm in diameter placed axially at the inlet of the burner. The central propane injector is surrounded by 5 orifices (0.75 mm in diameter) for injection of air. Downstream from the injector exit the diaphragm is placed. At 30 mm distance further downstream the gauze is set. The gauze cells are 1 mm in size. At the burner exit a grate and 3 gauzes are mounted. The grate has a few orifices 0.5 mm in diameter. Gauzes are turned relatively to one another at $\sim 30^\circ$ to obtain a stable flame. As a result of the burner construction, a stable flame that had a flat profile at a distance of 1–3 mm from the burner exit was realized. The gas was sampled at the burner axis of symmetry in the flame front and at 2 mm distance behind it. The air and propane mass flow rates were controlled independently in order to have a possibility of equivalence-ratio variation. The total mass flow rate did not exceed 0.5 g s^{-1}. The combustion products flowed out in ambient air.

The most frequently used technique to measure the ion and neutral species concentrations in flames is mass-spectrometry [7]. The technique is based on the extraction of a gas sample, ionization of the gas probe sampled and identification of ions using their deflection in an electromagnetic field. When detecting ions, the conventional mass-spectrometer is slightly modified, as ionization of the sampled charged particles is unnecessary. Here, a mass spectrometer of Balzers Quadstar QMS 421 type was used.

In order to minimize the influence of the gas sampling system on flame characteristics and composition of combustion products, the results related to the gasdynamic and thermal flame perturbations [19–22] were taken into account during system designing (material, orifice diameter, cone angle, etc.).

A water-cooled nickel cone 10 mm in length, with an aperture of 0.1 mm and an expansion angle of 60°, was used for gas sampling from a flame front. The cone was not cooled directly but it was mounted on the cooled base, placed at the head of the mass-spectrometer.

As soon as a molecular beam enters through the first pinhole with aperture $\emptyset_1 = 0.1$ mm into the acceleration zone of the extraction chamber, an isentropic expansion quenches, at least to some extent, chemical reactions. The second diaphragm ($\emptyset_2 = 0.4$ mm) set at 18 mm distance behind the first orifice samples the ion beam and gives access to the second chamber, where pressure falls down to $p_2 \sim 10^{-3}$ Torr. In the first extraction chamber the pressure is $p_1 \sim 5 \times 10^{-3}$ Torr but it decreases to $p_3 = 5 \times 10^{-6}$ Torr in the analyser region (see figure 1(*b*)).

Taking into account the influence of cone polarization on the spectra [23], the cone was grounded together with the flange of mass-spectrometer. The second and the third diaphragms ($\emptyset_2 = 0.4$ mm and $\emptyset_3 = 0.1$ mm) are polarized by external batteries in order to select and accelerate some kinds of ions. To detect positive ions the negative voltage typically of −7.5 V and −120 V has been applied to the second and the third diaphragms, respectively. To detect negative ions, these diaphragms were set in most cases at voltages of +8.3 V and +98 V, respectively. The voltages applied to electrical lenses $V_1 - V_5$ and V_8, were adjusted by the mass-spectrometer soft control in order to optimize the detector signal, i.e. to maximize the total ion current.

3. Theoretical model

A spatial temperature profile of the flat flame was calculated using the PREMIX code from the CHEMKIN software package [24] with species diffusion taken into account. It was estimated that the radiation heat transfer leads to minor temperature correction at the distance considered (∼10 K at the distance of 2 mm) behind the flame front. Therefore, the effect of flame radiation on the temperature profile was neglected. Estimations have demonstrated that processes involving charged species and soot particles do not affect the combustion kinetics and flow parameters. That is why the computed temperature profile was used for modelling of charged species evolution in flame with the detailed kinetic reaction mechanism of ion formation. The main disadvantage of this model is the neglect of diffusion in the equations describing plasma-chemical kinetics. This can result in much more sharp spatial profile of ion concentration in flame as compared with reality. The variation of gasdynamic parameters (temperature, pressure and gas velocity) during the extraction into the mass-spectrograph was estimated under the assumption of adiabatic flow expansion.

The kinetics of neutral species formation was based on the chemical reaction mechanism reported in [25], while the kinetics of ionic species during hydrocarbon/air combustion developed in [26] was extended in order to describe the generation of HCO_2^-, HCO_3^-, and $C_3H_7O^+$ ions observed in the present experiment. It is worth noting that the basic reaction mechanism of ion formation developed in [25] to study the charged species production during combustion of the methane-air mixture allows one to compute maximal concentrations of $C_2H_3O^+$ and H_3O^+ ions that is consistent with the experimental data for the methane-air flame reported in [6]. Additionally, the model was supplemented by the reactions of ion clusters formation (hydrated ionic clusters $H_3O^+{\cdot}(H_2O)_n$ ($n = 1, \ldots, 6$), $NO^+{\cdot}(H_2O)_m$ ($m = 1, \ldots, 3$), and others [27]) in the extraction system, when the gas probe temperature rapidly drops due to adiabatic expansion. The developed reaction mechanism involves more than 1300 reversible reactions with the participation of neutral species, ions, and ion clusters. Table 1 lists the main classes of the reactions with charged species involved in the model. The additional processes involved in the reaction mechanism [25, 26] to describe the HCO_2^-, HCO_3^-, and $C_3H_7O^+$ ionic species formation as well as coefficients for Archenius formula, $k^{+(-)} = A{\cdot}T^{n}{\cdot}\exp(-E_a/T)$, to estimate the forward (k^+) and backward (k^-) rate constants are listed in table 2. The coefficients A, n, E_a were taken from [28–30]. The rate constants for backward reactions for which the coefficients A, n, and E_a are not given in the table were calculated using the principle of detailed equilibrium. It should be mentioned that the rate constants for the cluster formation are known at rather narrow temperature range (243 K < T < 303 K) and a number of rate constants have strong temperature dependence. At lower temperature some estimated rate constants grow very rapidly with the temperature decrease and have non-physical values. So far, it was supposed that the rate constants of cluster formation at $T < 243$ K are equal to their values at $T = 243$ K. The equilibrium between vibrational, rotational and translational degrees of freedom of ions and molecules was assumed.

It is known that the combustion of hydrocarbon/air mixtures may produce soot particles even in the case of non-ideal flames close to the stoichiometric one. Until recently it was believed that soot particles formed during the combustion of hydrocarbon fuels are electrically neutral. However, recent experimental data [12] exhibited that soot particles, which are formed in a propane–air flame, may have a significant positive and negative charge, $Q = (5\text{–}10)\,e$, where e is the elementary charge. The modern theories of soot formation [31] cannot explain this phenomenon. According to [11] soot particles are polarized in ion produced electric field and may accumulate a significant charge on their surface due to attachment of various ions and electrons. The charging and discharging of soot particles in a bipolar ion environment can explain the observation [12]. Moreover, the charging of soot particles may decrease the total ion concentration in flame. That is why we have taken soot particle charging into account. As in [11], we have assumed that the size distribution of soot particles is lognormal

$$N_S(r) = \frac{N_S}{\sqrt{2\pi}\, r \ln(\sigma)} \exp\left[-\frac{1}{2}\left(\frac{\ln(r) - \ln(\bar{r})}{\ln \sigma}\right)^2\right].$$

Here N_S is the total concentration of soot particles, r is the radius of a soot particle, the mean radius $\bar{r}$ is 25 nm and geometrical deviation σ is 1.56 [31]. The detailed description of the model for ion-soot interaction is reported in [32].

4. Experimental results

The mass-spectra of ion content in stoichiometric propane/air laminar flame were investigated in flame front as well as at 2,

Table 1. List of main classes of the reactions with charged species.

Associative ionization	$A + B = AB^+ + e$
Dissociative ionization	$AB + e = A^- + B$
Ionization of atoms and molecules during interaction with an electron	$A + e = A^+ + e + e$
Associative attachment of an electron	$A + e + M = A + M$
Nonresonance recharging	$A^+ + B = A + B^+$
	$A^- + B = A + B$
Binary ion-molecular reactions	$AB^+ + CD = AC^+ + BD$
	$AB^- + CD = AC + BD$
Ion-molecular reactions with formation of an electron	$A^- + B = AB + e$
	$A^- + B = A + B + e$
	$AB^- + C = A^- + BC + e$
Ternary ion-molecular(atom) recombination	$A^+ + B + M = AB^+ + M$
	$A^- + B + M = AB + M$
Dissociative recombination	$AB^+ + e = A^- + B$
Ternary ion-electron recombination	$A^+ + e + M = A + M$
Ion–ion recombination	$A^- + B^+ = A + B$
	$A + BC^+ = A^- + B + C$
	$AB^- + C^+ = A + B + C$
Ternary ion–ion recombination	$A^- + B^+ + M = A + B + M$
	$A^- + B^+ + M = AB + M$
Formation of ionic clusters	$A^+(H_2O)_{n-1} + H_2O + M = A^+(H_2O)_n + M$
	$A^+ : H_3O^+, n = 1 \ldots 6; C_2H_3O^+, n = 1 \ldots 3;$
	$NO^+, n = 1 \ldots 3$
	$A^- + H_2O + M = A^-H_2O + M$
	$A^- : NO_3^-, NO_3^-HNO_3$
	$A^-(HNO_3)_{n-1} + HNO_3 + M = A^-(HNO_3)_n + M$
	$A^- : NO_3^-, n = 1 \ldots 5$
Ternary recombination of cluster and ion (or another cluster)	$A^+(H_2O)_n + B^-(HNO_3)_m + M = A + B + nH_2O + mHNO_3 + M$

5, and 10 mm distances downstream behind it. The obtained results allow the verification of the above described numerical model. Some general observations related to the performed measurements should be made.

First, the total ion current measured on the second diaphragm reaches a saturation value when a sufficient potential is applied to the flange (see figure 2(*a*)). Second, a value of the saturation current depends on the sign of the voltage applied to the flange and this value declines with the distance of the extraction from the flame front. The saturation current for positive voltage is lower than for negative one. It means that the concentration of positive ions is probably higher than the negative ions, at least when single charged ions prevail [22] in the studied regions of flame.

The positive and negative ion mass/charge spectra were recorded in the range from 0 to 512 atomic mass units (amu). Note that ions with mass above 100 amu have not been detected. The experimental data were averaged over 3–5 measurements. The results of mass-spectrometric measurements for stoichiometric propane/air flame are presented in figures 3 and 4 and summarized in table 3. Table 3 contains ion formulas, atomic mass units, and normalized peak intensities as well as information about the sampling region (flame front or burnt gas zone). The peaks in mass-spectra are related to the main positive (or negative) ions in the flame front or at 2 mm distance behind it.

Three main types of positive ions were identified in the flame front: $C_XH_Y^+$ as $C_3H_3^+$; $C_XH_YO^+$ as $C_2H_3O^+$, $C_3H_5O^+$, $C_3H_7O^+$; $H_XO_Y^+$ as H_3O^+. The major ion observed in the flame front was $C_2H_3O^+$ (see figure 3). This ion was found previously to be the most abundant ion in the stoichiometric methane–oxygen–argon flame at low pressure [22]. The observed spectra differ substantially from the spectra reported by Egsgard and Carlsen [33] for the flame front in propane/oxygen mixture, where H_3O^+ and $C_3H_3^+$ ions prevailed. However, the $C_2H_3O^+$ ion, mainly of the acetyl cationic structure (CH_3CO^+), was found to be second abundant in methane/oxygen flames in their later work [34].

The $C_3H_5O^+$ (57 amu) and $C_3H_7O^+$ (59 amu) ions have been mentioned in [2, 7]. Moreover, these ions were identified as methoxymethyl cation, $CH_3OCH_2^+$, and protonated dimethyl ether, $(CH_3)_2OH^+$, in flames of dimethyl ether with oxygen [35]. However, there might be also some contributions from hydrated $C_3H_3^+ \cdot H_2O$ and $C_3H_5^+ \cdot H_2O$ clusters to the respective peaks at 57 and 59 amu in the mass-spectra shown in figure 3. These clusters may form during the expansion of the gas probe in the extraction system.

When gas was sampled at 2 mm distance behind the flame front the ion composition was changed and the total ion concentration decreased. Several peaks of significant intensity were observed here, which correspond to the H_3O^+ (19 amu) ion and its hydrated clusters $H_3O^+ \cdot (H_2O)_n$ for $n = 1, 2, 3, 4$ with peaks at 37 amu, 55 amu, 73 amu and 91 amu, respectively. These clusters are rather unusual for plasma in flames at temperature of the order 2000 K. As will be demonstrated by the results of modelling these charged clusters may form during expansion of the gas probe in the extraction system. The H_3O^+ ions are produced by proton transfer from other ions (HCO^+, CH_3^+, $C_2H_3^+$, $C_3H_3^+$) to water molecules. There one can observe only another ion in burnt gas region in a significant quantity with 30 amu mass. It is NO^+ ion. The importance of this ion, when nitrogen compounds are present in a flame, was postulated by van Tiggelen [36] and was predicted by the computations in [26].

Table 2. List of additional chemical reactions with neutral and charged species describing the HCO_2^-, HCO_3^-, and $C_3H_7O^+$ ion formation and coefficients for calculation of rate constants (cm^3, mol, s, K).

No.	Reaction	k^+			k^-		
		A	n	E_a	A	n	E_a
1.	$C_3H_5+O_2 = CH_3COCH_2+O$	3.81×10^{17}	−1.36	2810	2.00×10^{11}	0	8812
2.	$iC_4H_7+O_2 = CH_3COCH_2+CH_2O$	7.14×10^{15}	−1.21	10600	1.23×10^{15}	−1.2	45416
3.	$CH_3CO+CH_3CHO = CH_3COCH_3+HCO$	1.71×10^{11}	0	0			
4.	$iC_3H_7+O = CH_3COCH_3+H$	4.82×10^{13}	0	0	1.29×10^{16}	−0.19	39973
5.	$iC_3H_7O = CH_3COCH_3+H$	2.00×10^{14}	0	10827	7.89×10^{12}	0.25	3429
6.	$iC_3H_7O+O_2 = CH_3COCH_3+HO_2$	9.09×10^{9}	0	196	1.00×10^{11}	0	16114
7.	$iC_3H_7O+NO = CH_3COCH_3+HNO$	3.92×10^{12}	0	196			
8.	$tC_4H_9+HO_2 = CH_3COCH_3+CH_3+OH$	1.81×10^{13}	0	0			
9.	$tC_4H_9+CH_3O_2 = CH_3COCH_3+CH_3O+CH_3$	1.21×10^{13}	0	0			
10.	$CH_3COCH_2 = CH_2CO+CH_3$	1.00×10^{14}	0	15610	1.00×10^{11}	0	3021
11.	$CH_3COCH_3 = CH_3CO+CH_3$	1.22×10^{23}	−1.99	42274	1.00×10^{13}	0	0
12.	$CH_3COCH_3+OH = CH_3COCH_2+H_2O$	1.05×10^{10}	0.97	799	6.93×10^{9}	0.97	11708
13.	$CH_3COCH_3+H = CH_3COCH_2+H_2$	5.63×10^{7}	2	3877	9.00×10^{12}	0	73016
14.	$CH_3COCH_3+O = CH_3COCH_2+OH$	1.13×10^{14}	0	3953	7.50×10^{12}	0	6194
15.	$CH_3COCH_3+CH_3 = CH_3COCH_2+CH_4$	3.96×10^{11}	0	4927	5.38×10^{8}	0.86	8832
16.	$CH_3COCH_3+CH_3O = CH_3COCH_2+CH_3OH$	1.00×10^{11}	0	3525	1.00×10^{10}	0	4532
17.	$CH_3COCH_3+C_2H_3 = CH_3COCH_2+C_2H_4$	1.23×10^{11}	0	2153			
18.	$CH_3COCH_3+C_3H_5 = CH_3COCH_2+C_3H_6$	7.08×10^{11}	0	8299	2.59×10^{10}	0	2273
19.	$CH_3COCH_3+O_2 = CH_3COCH_2+HO_2$	1.20×10^{14}	0	23164	2.00×10^{12}	0	1007
20.	$CH_3COCH_3+HO_2 = CH_3COCH_2+H_2O_2$	1.70×10^{13}	0	10303	1.00×10^{11}	0	4029
21.	$CH_3COCH_3+NO_2 = CH_3COCH_2+HNO_2$	3.80×10^{5}	0	3588			
22.	$H_3^++CH_3COCH_3 = C_3H_7O^++H_2$	2.59×10^{15}	0	0	0	0	0
23.	$H_3O^++CH_3COCH_3 = C_3H_7O^++H_2O$	2.35×10^{15}	0	0	0	0	0
24.	$HCO^++CH_3COCH_3 = C_3H_7O^++CO$	1.63×10^{15}	0	0	0	0	0
25.	$C_3H_7O^+ + e = CH_3CHO+CH_3$	9.03×10^{16}	−0.5	0	0	0	0
26.	$C_3H_7O^+ + e = CH_3COCH_3+H$	9.03×10^{16}	−0.5	0	0	0	0
27.	$CH_3^++CH_3CHO = C_3H_7O^+$	1.30×10^{13}	−0.66	0	0	0	0
28.	$C_3H_3O^+ + e = C_2H_3+CO$	1.81×10^{17}	−0.5	0	0	0	0
29.	$C_2H_3^+ + CO = C_3H_3O^+$	1.21×10^{9}	−2.5	0	0	0	0
30.	$HCO_3^-+H_3O^+ = CO_2+H_2O+H_2O$	6.02×10^{16}	0	0	0	0	0
31.	$OH^-+HCO = HCO_2^-+H$	2.46×10^{15}	0	0	0	0	0
32.	$CH_3CHO+OH = CH_3+HOCHO$	3.00×10^{15}	−1.08	0	5.35×10^{19}	−1.68	60326
33.	$OCHO+M = H+CO_2+M$	2.44×10^{15}	−0.5	13344	7.50×10^{13}	0	14603
34.	$HOCHO+M = CO+H_2O+M$	2.30×10^{13}	0	25178	1.42×10^{10}	0.46	23587
35.	$HOCHO+M = CO_2 + H_2+M$	1.50×10^{16}	0	28703	2.40×10^{14}	0.46	30727
36.	$HOCHO = HCO+OH$	4.59×10^{18}	−0.46	54535	1.00×10^{14}	0	0
37.	$CH_2O+OCHO = HCO+HOCHO$	5.60×10^{12}	0	6848	8.58×10^{11}	0.04	13470
38.	$OCHO+HO_2 = HOCHO+O_2$	3.50×10^{10}	0	−1649	3.70×10^{12}	−0.29	26533
39.	$OCHO+H_2O_2 = HOCHO+HO_2$	2.40×10^{12}	0	5036	1.79×10^{11}	0.36	12483
40.	$HOCHO+OH = H_2O+CO_2+H$	2.62×10^{6}	2.06	461	0	0	0
41.	$HOCHO+OH = H_2O+CO+OH$	1.85×10^{7}	1.51	−484	0	0	0
42.	$HOCHO+H = H_2 + CO_2+H$	4.24×10^{6}	2.1	2451	0	0	0
43.	$HOCHO+H = H_2 + CO+OH$	6.03×10^{13}	−0.35	1505	0	0	0
44.	$HOCHO+CH_3 = CH_4+CO+OH$	3.90×10^{-7}	5.8	1108	0	0	0
45.	$HOCHO+HO_2 = H_2O_2+CO+OH$	1.00×10^{12}	0	6002	0	0	0
46.	$HOCHO+O = CO+OH + OH$	1.77×10^{18}	−1.9	1498	0	0	0
47.	$O_2^-+HOCHO = HCO_2^-+HO_2$	2.46×10^{15}	0	0	0	0	0
48.	$HCO_2^-+HO_2 = HCO_3^-+OH$	1.00×10^{14}	0	0	0	0	0
49.	$HCO_2^-+H_3O^+ = HOCHO+H_2O$	6.02×10^{16}	0	0	0	0	0
50.	$HCO_2^-+NH_4^+ = HOCHO+NH_3$	6.02×10^{16}	0	0	0	0	0
51.	$HCO_2^-+A^+ = OCHO+A$ A=O_2, N_2, O, N, NO, NO_2, CO, CO_2, NH_3	2.09×10^{18}	−0.5	0	0	0	0
52.	$HCO_2^-+H^++M = HOCHO+M$	1.12×10^{29}	−2.5	0	0	0	0
53.	$HCO_2^-+A^++M = OCHO+A+M$ A=O_2, N_2, O, N, NO, NO_2	1.12×10^{29}	−2.5	0	0	0	0
54.	$HCO_3^-+A^+ = OCHO+AO$	2.09×10^{18}	−0.5	0	0	0	0
55.	$CO_3^-+A^+ = CO_2+AO$ A=O, N, NO, NO_2, CO	2.09×10^{18}	−0.5	0	0	0	0

It is worth noting that as we proceed with gas extraction downstream in the burnt gas region (5 and 10 mm distance behind flame front) the ion current decreases (see e.g. figure 2(*b*)). Nevertheless, the same main ionic species are continuously observed, i.e. the H_3O^+, NO^+ ions and $H_3O^+\cdot(H_2O)_n$ clusters.

The identification of some negative ions observed in the flame front and in the post front region presents some diffi-

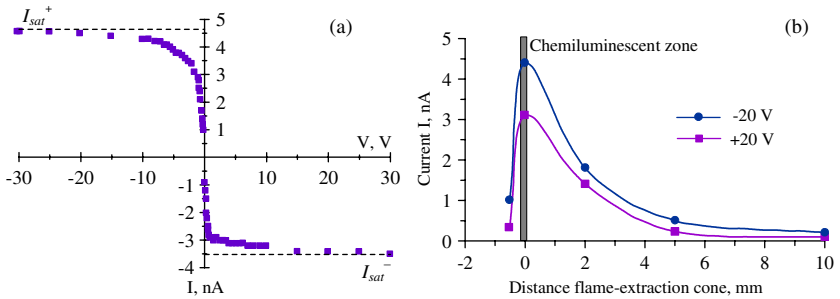

Figure 2. The total ion current, I, measured on the second diaphragm of extraction system versus the flange voltage (*a*) and distance from the flame front (*b*).

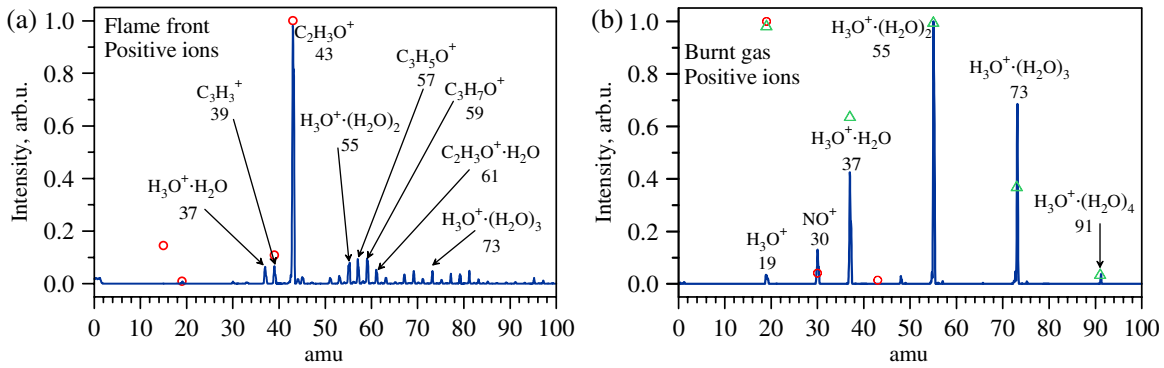

Figure 3. Mass-spectra of positive ions extracted in flame front (*a*) and 2 mm behind it (*b*).

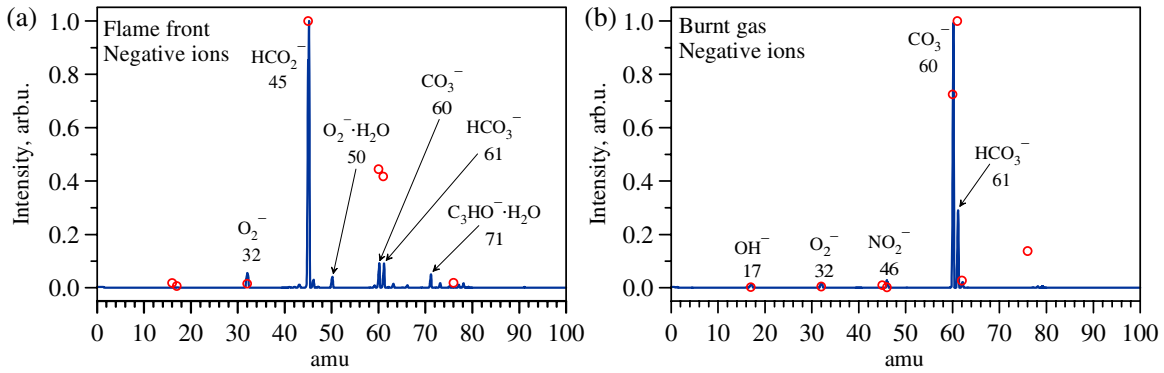

Figure 4. Mass-spectra of negative ions extracted in flame front (*a*) and 2 mm behind it (*b*).

culty, as the related literature is more limited. In the work on a low pressure methane/oxygen flame, Feugier and van Tigge-len [37] reported the prevalence of the OH^-, O^- and CH_3^- ions. These ions are only of minor importance in our measurements (see figure 4 and table 3).

The presented results are much closer to the findings of Goodings *et al* [38] for stoichiometric methane/oxygen flame, with the prevailing HCO_2^- (45 amu) and CO_3^- (60 amu) ions. These researches also observed the other ions: O_2^- (32 amu), $C_2H_3O^-$(43 amu), OH^- (17 amu), C_6H^- (73 amu) and C_2H^- (25 amu) in fuel rich CH_4/O_2 flame and they postulated O_2^- as the primary negative ion. The results obtained earlier in [39] agree quite well with the data in table 3, at least for the most abundant negative ions (in decreasing order of concentration): HCO_2^-, CO_3^-, HCO_3^- and O_2^-.

Only, negligible concentrations of negative ions containing nitrogen can be traced at 59 amu ($HCNO_2^-$) and even less abundant at 42 amu (CNO^-) or at 62 amu (NO_3^-).

No ion formulas have been found in the literature for ions with mass of 50 and 71 amu. Most probably they can be assigned as hydrated ionic clusters: $O_2^-\cdot H_2O$ [40] and $C_3HO^-\cdot H_2O$, respectively. The ion C_3HO^- with mass of 53 amu was identified by Fontijn and Miller [39] at low pressure acetylene/oxygen flames.

The observed ions are typically multi-oxygenated. Again, just a few negative ions persist in the burnt gas region behind the flame front (see figure 4(*b*) and table 3).

5. Model verification for the stoichiometric propane/air mixture

The mass-spectra of ions measured in the flame-front and at 2 mm distance downstream have been used to verify the model presented here. Figure 5 shows the calculated spatial profiles of temperature and ion mole fractions in the stoichiometric propane/air flame (fuel/air equivalence ratio $\varphi = 1.0$), under

Table 3. Relative intensities of main positive and negative ions in flame front and 2 mm behind it during combustion of stoichiometric propane/air mixture.

Ion charge	Mass, amu	Formula	Peak intensity, relative units	Sampling cross-section
	37	$H_3O^+ \cdot H_2O$	0.065	
	39	$C_3H_3^+$	0.067	
	43	$C_2H_3O^+$	1	
Positive	55	$H_3O^+ \cdot (H_2O)_2$	0.08	Flame front
	57	$C_3H_5O^+$ or $C_3H_3^+ \cdot H_2O$	0.093	
	59	$C_3H_7O^+$ or $C_3H_5^+ \cdot H_2O$	0.097	
	61	(probably) $C_2H_3O^+ \cdot (H_2O)$	0.052	
	73	$H_3O^+ \cdot (H_2O)_3$	0.019	
	19	H_3O^+	0.035	
	30	NO^+	0.132	2 mm distance
Positive	37	$H_3O^+ \cdot H_2O$	0.427	behind
	55	$H_3O^+ \cdot (H_2O)_2$	1	flame front
	73	$H_3O^+ \cdot (H_2O)_3$	0.687	
	91	$H_3O^+ \cdot (H_2O)_4$	0.037	
	32	O_2^-	0.055	
	45	HCO_2^-	1	
Negative	50	$O_2^- \cdot H_2O$	0.042	Flame front
	60	CO_3^-	0.093	
	61	HCO_3^-	0.092	
	71	$C_3HO^- \cdot H_2O$	0.051	
	17	OH^-	0.013	
	32	O_2^-	0.016	2 mm distance
Negative	46	NO_2^-	0.029	behind
	60	CO_3^-	1	flame front
	61	HCO_3^-	0.29	

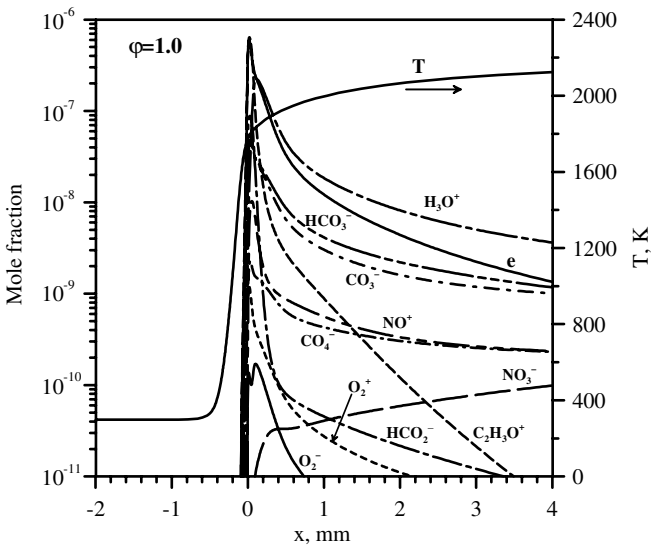

Figure 5. Predicted spatial profile of ion mole fractions and temperature in stoichiometric propane/air atmospheric pressure flame.

the assumption of absence of soot particles ($N_S = 0$). Here, the centre of a flame front (defined as the position of maximal concentration of CH radicals) is placed at $x = 0$, and the distance downstream behind the flame front is actually calculated from that point (i.e. the thickness of the flame front has not been taken into account).

One sees that the positive ions $C_2H_3O^+$ and negative ions HCO_2^- prevail in the flame front in a good agreement with the experimental data. These ions are the most abundant among positive and negative ions, respectively. The concentrations of CO_3^- and HCO_3^- ions are much smaller than that of HCO_2^-. The H_3O^+ ions are considerably less abundant than $C_2H_3O^+$ ones in the flame front. The concentration of $C_3H_3^+$ ions is quite low (both in experimental and in simulation results), in contrast to observed concentration values in [34, 36]. It does not exceed 10% of the main ion ($C_2H_3O^+$) concentration and its evolution is very rapid. It practically disappears at 0.1 mm distance behind the flame front. Moreover, it was already pointed out by Fialkov [7] that this ion can play a significant role only in fuel-rich flames. It should be noted that the computed decay length of ion concentration is smaller than that detected in experiment. This disagreement may be caused by the uncertainty in the mixture flow rate, which was not measured in experiments. In our computations we assumed that flow rate is equal to $0.5\,g\,s^{-1}$. An increase in the value of the flow rate to $1\,g\,s^{-1}$ reduces significantly the difference between calculated and observed values of ion concentration decay length. The other reason for the disagreement in the predicted and observed decay length for charged species is the neglect of the diffusion of ions and electrons that concentrations in the flame front region are maximal.

Slightly, behind the flame front, the H_3O^+ becomes the main ion in the flame due to the fast decay of $C_2H_3O^+$. Actually, at 2 mm distance downstream from the flame front H_3O^+ and NO^+ ions present more than 97% of ion population in agreement with experiment. This estimation takes into account that hydrated clusters, $H_3O^+ \cdot (H_2O)_n$, are formed from H_3O^+ during rapid cooling in the extraction system of mass-spectrometer (see figure 6(*b*)).

The dynamics of cluster formation is clearly seen in figure 6 which depicts the evolution of temperature and ion mole fractions along the extraction system. A significant amount of $H_3O^+ \cdot (H_2O)_n$ ionic clusters forms in the extraction system, with $H_3O^+ \cdot (H_2O)_2$ prevailing in accordance with

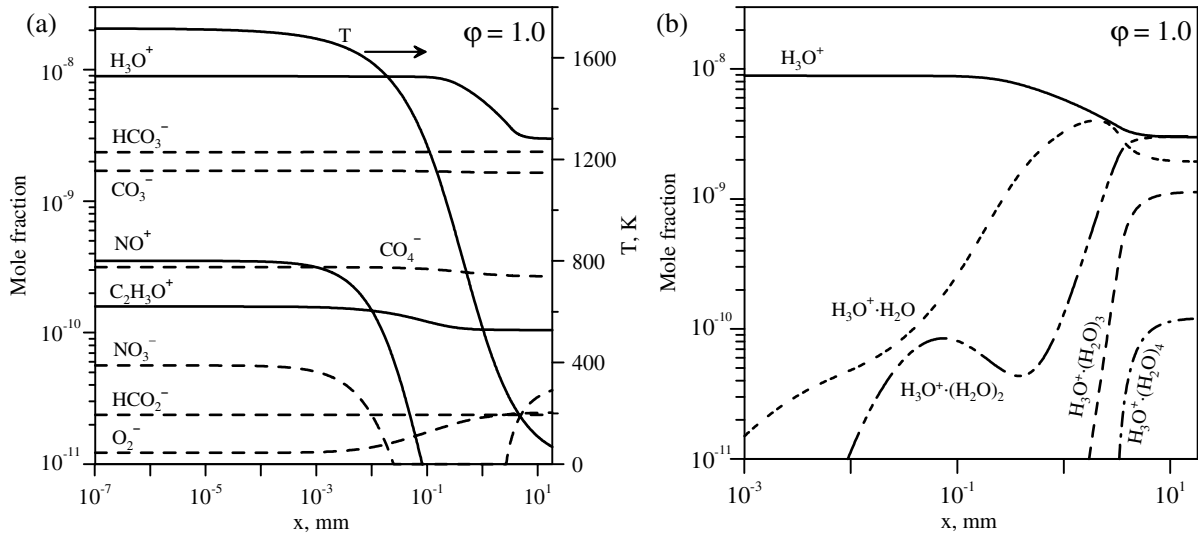

Figure 6. Predicted spatial distribution of temperature and ion mole fractions (*a*) as well as mole fractions of hydrated H_3O^+ clusters (*b*) in extraction system for gas sampled at 2 mm behind the flame front of stoichiometric propane/air mixture at atmospheric pressure.

measurements. The good agreement can be observed also for CO_3^- and HCO_3^- ions, which remain the main negative ions at 2 mm distance behind the flame front. It should be mentioned, however, that we could not reproduce properly the evolution of $C_2H_3O^+$ion concentration in the extraction system. The predicted $C_2H_3O^+$ concentration falls rather rapidly during the expansion of gas probe in the extraction nozzle.

The main source of observed discrepancies is related to limitations of the model, namely, at the temperature below 200–250 K and low pressure in the extraction system where there is no equilibrium between rotational and translational degrees of freedom for ions and molecules. So, the rate constants for different processes are not defined properly in this temperature range. This includes also the formation of different ionic clusters. Moreover, to obtain quantitative agreement, a number of factors like experimental temperature profile along the flame and temperature evolution during gas expansion in the extraction system must be known. Nevertheless, the simulation results of ion composition correlate reasonably well with the experimental data—see figures 3 and 4. It should be pointed out that both in experiment and theory the $C_2H_3O^+$ ions prevail in the flame front. Besides as shown by triangles, Δ and circles, $\circ$, in figure 4(*a*), the experimentally observed hydrated ions $H_3O^+{\cdot}(H_2O)_n$ stem from the H_3O^+ one. Besides, from our calculation we conclude that most probably the $C_3H_5O^+$ ion should be related to the hydrated $C_3H_3^+{\cdot}H_2O$ cluster-ion. Relatively good agreement is found for negative ions. Special attention should be paid to a shift from HCO_2^- to CO_3^- and HCO_3^- as we move from the results in flame-front to the one 2 mm behind the front.

Besides, we want to point out that our experimental and theoretical spectra agree well with the data of other researchers, see e.g. [6,22,34] in relation to the most prevalent ion $C_2H_3O^+$ and H_3O^+; [2, 7, 35] in relation to the $C_3H_5O^+$ ($C_3H_3^+{\cdot}H_2O$) ions; [36] in relation to the NO^+ ion; [38, 39] in relation to the HCO_2^- and CO_3^- ions; [39] in relation to the HCO_3^- ions. These ions have been also found to prevail in our theoretical studies.

Figure 7(*a*) presents the spatial profiles of temperature as well as total negative and positive ion concentrations at $\phi = 1.0$. One sees that the region of significant ion concentration is localized closely to the flame front and this zone is about 0.5 mm in thickness. The ion concentration drops rather rapidly with distance from flame front in agreement with the experimental data. The maximum of total concentration of positive ions observed in the flame front zone shifts slightly that for negative ones (a few μm), most probably due to time needed for attachment processes to produce negative ions. This is in a qualitative agreement with the data presented in [41] for a low pressure acetylene/oxygen flame, where the positive ion concentration peaks were observed at the centre of the flame front zone and the negative ion concentration peaks were located further downstream. However, our results differ from those of Knewstubb [41] obtained for fuel-rich acetylene flame at 1 bar pressure, where the negative ions were observed only close to the flame front and much earlier than the positive ones. Figure 7(*b*) shows spatial profiles of positive ions for different fuel/air equivalence ratios. The profile width and height increase with ϕ at least in the range $0.7 < \phi < 1.15$.

Finally, we should explain the difference in the total positive and negative ion concentrations, i.e. a domination of saturation current measured on flange (see figure 2), when a negative voltage is applied. This phenomenon can be explained by plasma-wall and ion-soot interactions. It is well known that the electron current prevails on any earthed metal surface placed in quasi-neutral plasma due to differences in electron and ion mobility. This may lead to a substantial decay of negatively charged species in a plasma-metal interface.

In what follows, we have also estimated the influence of the ion-soot interaction on the gas plasma quasi-neutrality. Figure 8 depicts the predicted spatial profile of the total positive ion (N_i^+) and negative species (ions+ electrons) concentrations (N_i^-) along the flame for various concentration of soot particles N_S. In propane/air flames the N_S value can vary from 10^7 to 10^{10} cm^{-3}, depending on fuel/air equivalence ratio value. Because there was no experimental information about the N_S value for the studied stoichiometric propane/air flame, the computations have been carried out for $N_S = 0; 10^7; 10^8$ cm^{-3}.

If the soot particle concentration is smaller than 10^7 cm^{-3}, the total concentrations of negatively and positively charged

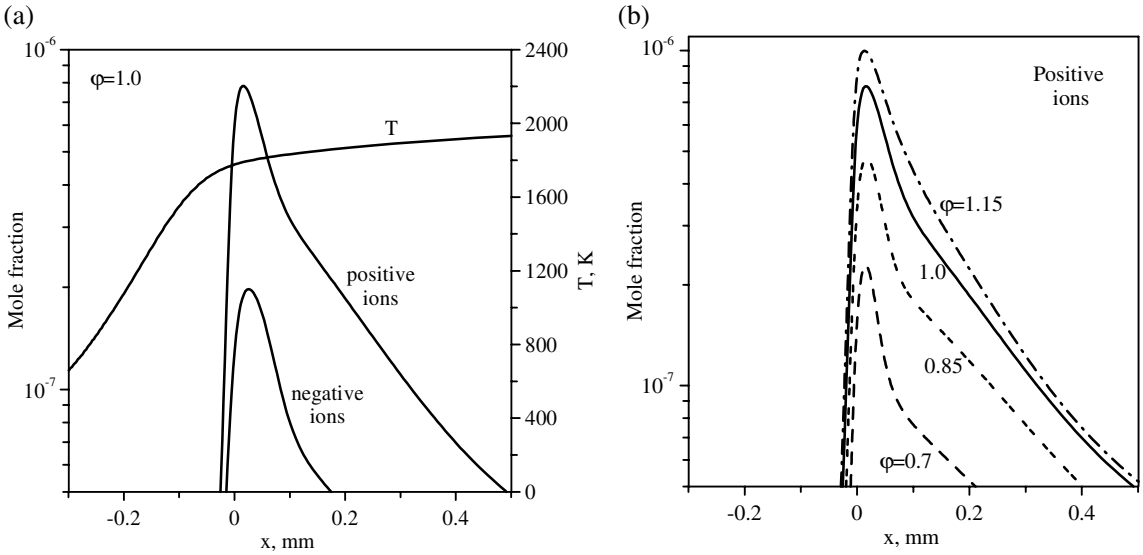

Figure 7. Spatial profiles of temperature as well as total negative and positive ion mole fractions at different φ values.

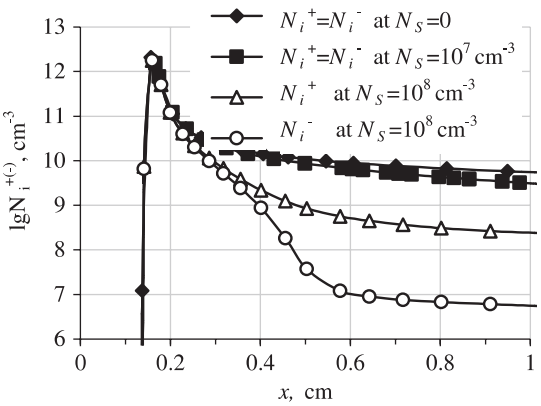

Figure 8. Predicted evolution of gaseous charged species concentration along the stoichiometric propane/air flame at different values of N_s.

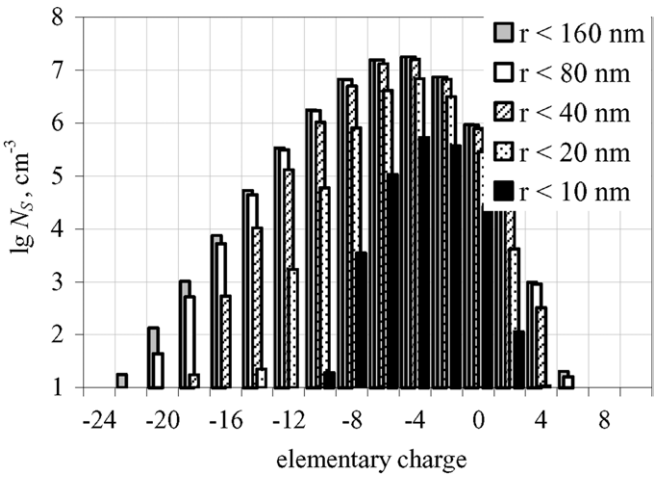

Figure 9. Charge distribution of soot particles with different radius at 7.6 mm distance behind the flame front.

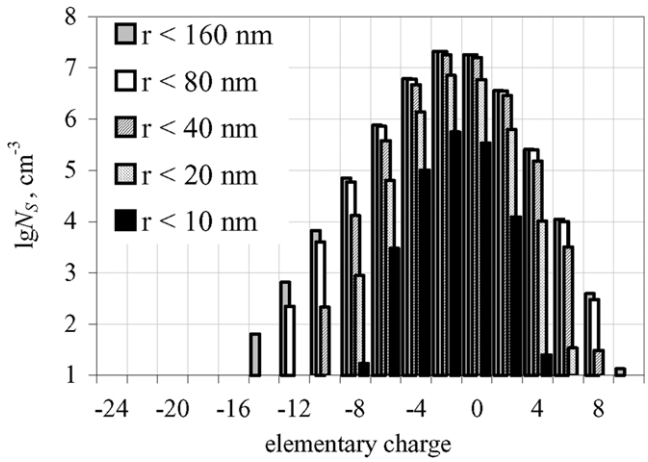

Figure 10. Charge distribution of soot particles with different radius at 25 mm distance behind the flame front.

gaseous species are approximately equal. But at $N_S = 10^8$ cm^{-3} one sees the difference between (N_i^+) and (N_i^-), which starts at 1 mm distance behind the flame front. The concentration of negatively charged gaseous species is essentially smaller than that of positive ones. The main reason for this is again related to the larger mobility of prevailing negatively charged species (i.e. electrons) compared with the mobility of main positive ions ($C_2H_3O^+$ or H_3O^+). It results in a faster rate for attachment of negatively charged species to soot particles than that for positive ions. So, the majority of soot particles are charged negatively. As a result the total concentration of negatively charged species becomes smaller than the one for positive ions. By increasing the N_S value the difference between concentrations of negative and positive ions increases.

Figure 9 depicts the charge distribution of soot particles with different radius at 7.6 mm distance from the flame front. Large particles (with radius of about 80 nm) may accumulate 10–20 elementary charges, whereas small particles ($r \sim 10$ nm) may acquire 6–8 elementary charges only. Due to the larger rate for attachment of negatively charged species to soot particles the distributions is asymmetrical, shifted towards negative cumulative charge. However, at larger distances the charge distribution becomes more symmetrical. The concentration of negatively charged particles is much lower there (see figure 8), as far as the attachment rates of positively

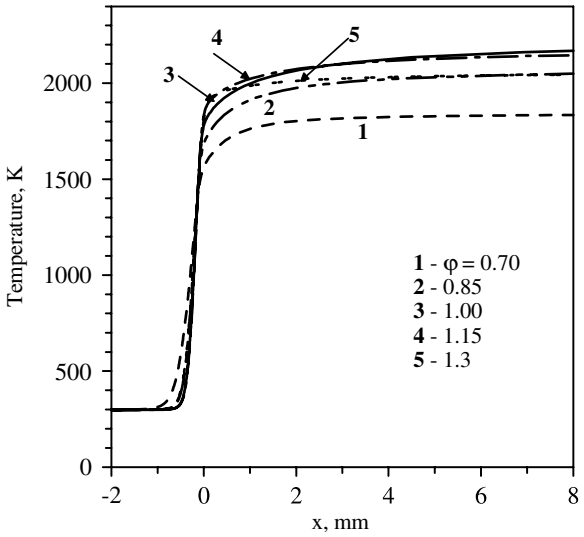

Figure 11. Predicted spatial profiles of temperature in propane/air flames with different φ values.

and negatively charged species to soot particles equalize (see figure 10).

6. Dependence of ion concentration on fuel/air ratio

Figure 11 shows the predicted spatial profiles of gas temperature for mixtures with equivalence ratio $\varphi = 0.7$, 0.85, 1.0, 1.15 and 1.3. One finds that the temperature growth begins at 1 mm distance the flame front upstream for the fuel lean mixture ($\varphi = 0.7$) and about 0.5 mm distance further for other mixtures (for $\varphi = 1.3$, 0.85, 1.0 and 1.15). Later, the temperature gradient for mixtures with $\varphi = 1.15$ and 1.3 is largest and shortly before the flame-front all profiles join together at temperature ∼1400 K. In a flame front the value of the temperature grows with increasing φ value and the difference in the temperature behind the flame front exceeds 300 K for the most fuel lean and fuel rich mixtures considered. In the post flame front region the temperature profiles exhibit saturation behaviour and this starts first for the most fuel lean and fuel rich mixtures ($\varphi = 0.7$ and 1.3). At 2 mm distance behind the flame front the temperature is not any more a monotonic function of the equivalence ratio but it attains the maximal value for φ range from 1.0 to 1.15. It is worth noting that the temperature behind a flame front is overestimated due to the neglect of the radiation heat transfer as discussed above. The overestimation increases with a distance from the flame front and can exceed even 100 K at a few centimetres distance behind the front.

Figures 12(*a*)–(*d*) presents the predicted spatial profiles of the main ionic species ($C_2H_3O^+$, H_3O^+, HCO_2 and CO_3^-) for different φ values and figure 13 shows the dependence of maximal concentration (and concentration at 2 mm distance behind the flame front) of ionic species as a function of the equivalence ratio. In the case of the main ionic species $C_2H_3O^+$, its maximal concentration, $[C_2H_3O^+]_{max}$, practically increases with the equivalence ratio increasing in the considered range of φ (see figure 13(*a*)). However, the value of $C_2H_3O^+$ concentration falls down rapidly just behind the flame front. At 1 mm distance behind the front the $C_2H_3O^+$ concentrations are much smaller than 1% of their initial values and the rate of the fall decreases with the growth of the equivalence ratio (see figure 12(*a*)).

At 2 mm distance behind the flame front the concentrations of this ion are ∼ 3 or 4 orders of magnitude lower than the initial values (see figure 13(*b*)). At larger distances, the concentrations saturate (except in the case of stoichiometric mixture) but at a rather low level. In contrast, the $[H_3O^+]_{max}$ has a pronounced maximum for the stoichiometric mixture (figure 13(*a*)) and falls drastically for fuel rich mixtures. H_3O^+ becomes the main ion for $\varphi = 0.7$ at 1 or 2 mm distance behind the flame front. Conversely, the roles of the $C_2H_3O^+$ and $C_3H_3^+$ ions increase in the fuel rich flame front. One sees in figure 12(*b*) that the spatial profiles of H_3O^+ do not differ substantially (besides peak value) for all mixtures considered. The concentration falls down (quasi-exponentially) to a value of 1–2% of its maximal value at the distance of 8 mm behind the flame front.

Figure 13(*a*) presents the dependence of maximal ion concentrations as a function of the equivalence ratio for other quite important ions absent in figure 5 due to their very fast decay, i.e. $[CH_3^+]_{max}$ and $[C_3H_3^+]_{max}$. The first, $[CH_3^+]_{max}$, slowly decreases with the increasing equivalence ratio (although a slight maximum for φ∼1.15 can be traced). On the contrary, $[C_3H_3^+]_{max}$ practically increases with φ value increasing, as already pointed out in [7]. Due to their fast decay, these ions (and to a lesser degree $C_2H_3O^+$) are especially hard to observe as the flame instabilities may strongly influence the measured concentrations.

The dependence on equivalence ratio of main nitrogen containing ion NO^+ is somehow similar to $H_3O^+$and its relative importance grows with the distance (downstream) from the flame front that has been observed in [2].

In the flame front the main negative species are electrons and their role increases with the equivalence ratio growth (see figure 13(*b*)). HCO_2^- and CO_3^- ions constitute only a minor contribution in flame front and their role decreases for fuel rich mixtures. One sees that the second negative ion CO_3^- becomes most important at a few millimetres distance behind the front, especially at fuel lean mixtures.

7. Concluding remarks

The computed and experimental results exhibit that ion composition of propane/air stoichiometric flame strongly depends on the distance from the flame front. The proposed kinetic model of ion formation in propane/air atmospheric pressure flame helps to understand the peculiarities of ion formation tendencies and is in a qualitative agreement with experimental data.

The most abundant charged species in the flame front region for stoichiometric propane/ air mixture are $C_2H_3O^+$, HCO_2^- ions and electrons. By increasing the distance from the flame front the ion composition changes significantly. In the burnt gas region the major charged species are H_3O^+, NO^+, CO_3^-, HCO_3^- ions and electrons. The concentration of $C_2H_3O^+$, HCO_3^- ions and electrons grows by increasing the equivalence ratio. In contrast, the importance of H_3O^+, NO^+ and CO_3^- ion grows with the distance from the flame front. The ionic clusters $H_3O^+(H_2O)_n$, $n = 1, \ldots, 4$, which were

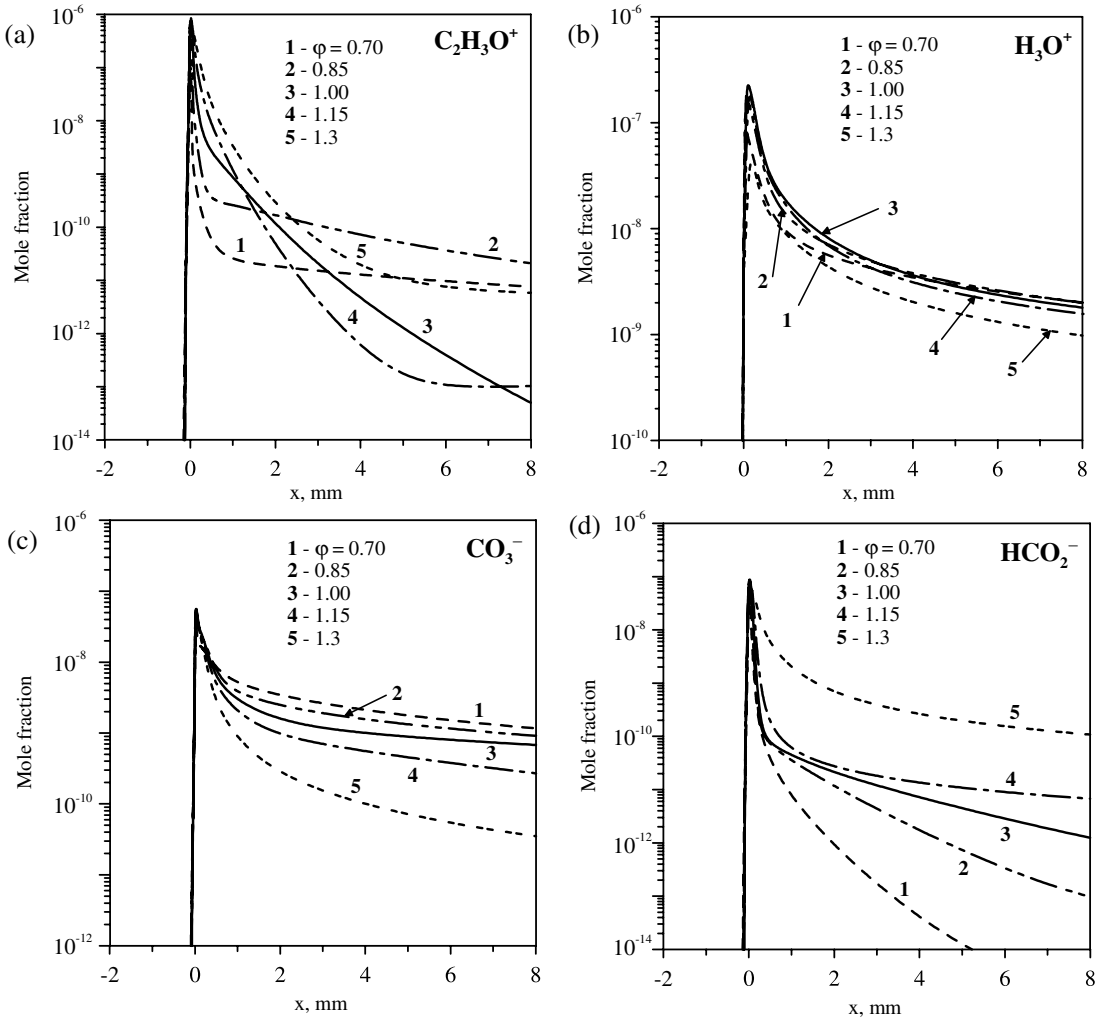

Figure 12. Predicted spatial profiles of main positive and negative ions at different φ values.

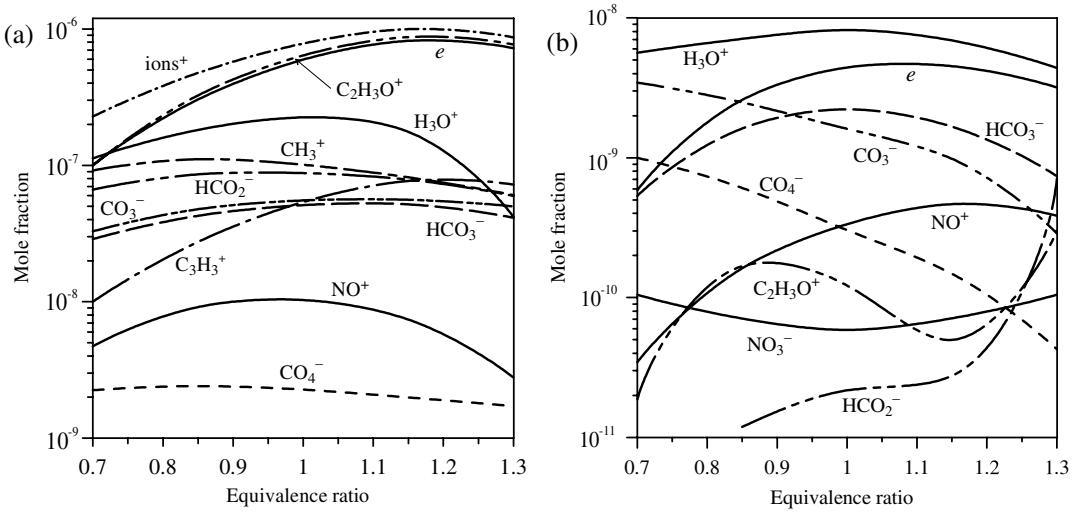

Figure 13. Predicted maximal values of positive and negative ion mole fractions (*a*) and their values at 2 mm distance behind flame front (*b*) as a function of equivalence ratio.

observed experimentally, probably form during the adiabatic expansion in the extraction system. The difference between concentrations of positively and negatively charged species observed in experiment may be explained by electron flux to the metal surfaces and by attachment of ions and electrons to soot particles.

For a quantitative description of experimental results, more detailed experimental data are required, especially on temperature evolution along the flame. Special attention should be paid to the measurement perturbation by a flame quenching-zone near the first pinhole as well as by the whole extraction system (including gas-cooling effects).

Acknowledgments

The work was sponsored by the bilateral Belgian–Polish and Belarus–Polish cooperation programmes and the 4T10B 01922 Project of Polish Committee for Scientific Research. The work was also supported by the Russian Foundation for Basic Research (Grants: 040333162 and 05-01-00355) and the Council of the President of the Russian Federation for Support of Young Russian Scientists and Leading Scientific Schools (Grant SS-9330.2006.8).

References

[1] Böhme D K 1972 Chemical ionization in flames *Ion Molecular Reactions* (New York: Plenum) pp 323–43
[2] Hayhurst A N and Kittelson D B 1978 *Combust. Flame* **31** 37–51
[3] Gooding J M, Böhme D K and Ng C-W 1979 *Combust. Flame* **36** 45–62
[4] Eraslan A N and Brown R C 1988 *Combust. Flame* **74** 19–37
[5] Calcote H F and Keil D G 1990 *Pure Appl. Chem*. **62** 815–24
[6] Pedersen T and Brown R C 1993 *Combust. Flame* **94** 433–48
[7] Fialkov A B 1997 *Prog. Energy Combust. Sci.* **23** 399–528
[8] Weilmuster P, Keller A and Homann K-H 1999 *Combust. Flame* **116** 62–83
[9] Starik A M, Savel'ev A M, Titova N S and Schumann U 2002 *Aerospace Sci. Technol*. **6** 63–81
[10] Haverkamp H, Wihem S, Sorokin A and Arnold F 2004 *Atmos. Environ.* **38** 2879–84
[11] Savel'ev A M, Starik A M, Titova N S and Favorskii O N 2004 *Dokl. Phys.* **49** 441–6
[12] Onischuk A A *et al* 2003 *J. Aerosol Sci.* **34** 383–403
[13] Yu F and Turco R P 1998 *J. Geophys. Res.* **103** 25915–34
[14] Fahey D W, Shumann U, Ackerman S, Artaxo P, Boucher O, Danilin M Y, Kärcher B, Minnis P, Nakajima T and Toon O B 1999 *Aviation and the Global Atmosphere, A Special Report of IPCC (Intergovernmental Panel on Climate Change)*, ed J E Penner *et al* (Cambridge: Cambridge University Press) pp 65–120
[15] Starik A M, Savel'ev A M and Titova N S 2005 *Proc. 2nd Int. Workshop on Cold Atmospheric Pressure Plasmas: Sources and Applications (Bruges, Belgium)* pp 118–122
[16] Yoshimaya S and Tomita E 2000 Fundamental study on combustion diagnostics using a spark plug as an ion probe *SAE Paper* 2000-01-2828
[17] Sotton J, Labuda S A, Ruttun B and Bellenoue M 2004 *30th Int. Symp. on Combustion*, W-I-P p 241
[18] Bellenoue M, Cenian A, Kageyama T, Labuda S A and Leys C 2003 *J. Tech. Phys.* **44** 363
[19] Hayhurst A N and Telford N R 1977 *Combust. Flame* **28** 67
[20] Hayhurst A N, Kittelson D B and Telford N R 1977 *Combust. Flame* **28** 123
[21] Hayhurst A N and Kittelson D B 1977 *Combust. Flame* **28** 137
[22] Biordi J C 1977 *Prog. Energy Sci.* **3** 151–73
[23] Axford S D T, Goodings J M and Hayhurst A N 1998 *Combust. Flame* **114** 294–302
[24] Kee R J *et al* 2004 *CHEMKIN Release* 4.0, Reaction Design, Inc., San Diego, CA
[25] Starik A M, Titova N S and Yanovsky L S 1999 *Kinetics Catal.* **40** 11–26
[26] Starik A M and Titova N S 2002 *Combust. Explosion Shock Waves* **38** 253–68
[27] Starik A M, Savel'ev A M, Titova N S, Loukhovitskaya E E and Schumann U 2004 *Phys. Chem. Chem. Phys.* **6** 3426–36
[28] Le Teuff Y H, Millar T J and Markwick A J 2000 *Astron. Astrophys. Suppl. Ser.* **146** 157–68
[29] Mallard W G, Westley F, Herron J T and Hampson R F 1994 *NIST Chemical Kinetics Database* -Version 6.0, NIST Standard Reference Data, Gaithersburg, MD
[30] http://www-cms.llnl.gov/combustion/combustion_home.html
[31] Bockhrom H ed 1994 *Soot formation in combustion* (Berlin: Springer)
[32] Savel'ev A M and Starik A M 2006 *Tech. Phys.* **4** 444–52
[33] Egsgaard H and Carlsen L 1993 *J. Anal. Appl. Pyrol.* **25** 361–70
[34] Egsgaard H and Carlsen L 1995 *Chem. Phys. Lett.* **236** 78–82
[35] Østergaard L F, Egsgaard H and Hammerum S 2003 *Phys. Chem. Chem. Phys.* **5** 3126
[36] Van Tiggelen A 1963 *Prog. Astronaut. Aeronaut.* **12** 165
[37] Feugier A and Van Tiggelen A 1965 *10th Symp. on Combustion* (Pittsburgh: The Combustion Institute) p 621
[38] Goodings J M, Bohme D K and Sugden T M 1976 *16th Symp. on Combustion* (Pittsburgh: The Combustion Institute) p 891
[39] Fontijn A and Miller W J 1965 *10th Symp. on Combustion* (Pittsburgh: The Combustion Institute) p 623
[40] Hayhurst A N 2005 private communication.
[41] Knewstubb P F 1965 *10th Symp. on Combustion* (Pittsburgh: The Combustion Institute) p 623

AQ2

QUERIES

Page 1

AQ1

“Please be aware that the color figures in this article will only appear in colour in the web version. If you require colour in the printed journal and have not previously arranged it, Please contact the Production Editor now.”

Page 12

AQ2

Please provide the place of symposium for the refs [17,37–39,40].